TITLE PAGE

Submission date: 15.11.2001

Word count: 7497

Pile monitoring during axial compression, pullout and flexure test using fiber optic sensors

Dr. Branko Glisic, Solutions & Services Manager, SMARTEC SA, Via Pobbiette 11, 6928 Manno, Switzerland, Phone: +41 91 610 18 00, Fax: +41 91 610 18 01, glisic@smartec.ch

Dr. Daniele Inaudi, CTO, SMARTEC SA, Via Pobbiette 11, 6928 Manno, Switzerland, Phone: +41 91 610 18 00, Fax: +41 91 610 18 01, inaudi@smartec.ch

Claire Nan, Executive Vice President, RouteAero Tech. & Eng., 12F-1, 56 Nanking E. Road, Sec. 5, Taipei 105, Taiwan, R.O.C, Phone: +886 (2) 2747 1055, Fax: +886 (2) 2747 1052, claire_nan@routeaero.com.tw

ABSTRACT

A full-scale on-site test represents an ideal way to check hypothesis and to determine the real behavior of structures, especially in cases where some uncertainties cannot be reduced otherwise. To perform the test successfully it is necessary to monitor the parameters that representatively describe the structural behavior. In the case of piles, an axial compression, pullout and flexure tests cover all load combinations that may appear in service. To assess the foundations performance a semiconductor production facility, two sets of piles with three piles in each set were tested. The monitored parameters were average strains, registered in several segments over the whole length of each pile using long-gage fiber optic sensors. This type of sensor, combined in appropriate topologies gives rich information concerning the piles behavior and soil properties. The aim of this paper is to present the monitoring method and to discuss its performances through the results of the tests. This method allowed the determination of the Young modulus of the piles, the occurrence of cracks, the normal force distribution, the ultimate load capacity in case of axial compression and pullout tests as well as the curvature distribution, horizontal displacement, deformed shape and damage localization in case of the flexure tests. Moreover the pile-soil friction distributions, the quality of soil and the pile tip force were estimated. The advantage of the presented method resides in the use of long-gage sensors, which are insensitive to local structural defects like crack openings or air pockets, and allow the collection of data on a global structural level and not on local, material level.

Pile monitoring during axial compression, pullout and flexure test using fiber optic sensors

Dr. Branko Glisic, Solutions & Services Manager, SMARTEC SA, Via Pobbiette 11, 6928 Manno, Switzerland, Phone: +41 91 610 18 00, Fax: +41 91 610 18 01, glisic@smartec.ch
Dr. Daniele Inaudi, CTO, SMARTEC SA, Via Pobbiette 11, 6928 Manno, Switzerland, Phone: +41 91 610 18 00, Fax: +41 91 610 18 01, inaudi@smartec.ch
Claire Nan, Executive Vice President, RouteAero Tech. & Eng., 12F-1, 56 Nanking E. Road, Sec. 5, Taipei 105, Taiwan, R.O.C, Phone: +886 (2) 2747 1055, Fax: +886 (2) 2747 1052, claire_nan@routeaero.com.tw

Abstract. A full-scale on-site test represents an ideal way to check hypothesis and to determine the real behavior of structures, especially in cases where some uncertainties cannot be reduced otherwise. To perform the test successfully it is necessary to monitor the parameters that representatively describe the structural behavior. In the case of piles, an axial compression, pullout and flexure tests cover all load combinations that may appear in service. To assess the foundations performance a semiconductor production facility, two sets of piles with three piles in each set were tested. The monitored parameters were average strains, registered in several segments over the whole length of each pile using long-gage fiber optic sensors. This type of sensor, combined in appropriate topologies gives rich information concerning the piles behavior and soil properties. The aim of this paper is to present the monitoring method and to discuss its performances through the results of the tests. This method allowed the determination of the Young modulus of the piles, the occurrence of cracks, the normal force distribution, the ultimate load capacity in case of axial compression and pullout tests as well as the curvature distribution, horizontal displacement, deformed shape and damage localization in case of the flexure tests. Moreover the pile-soil friction distributions, the quality of soil and the pile tip force were estimated. The advantage of the presented method resides in the use of long-gage sensors, which are insensitive to local structural defects like crack openings or air pockets, and allow the collection of data on a global structural level and not on local, material level.

INTRODUCTION

A new semi-conductor production facility in the Tainan Scientific Park, Taiwan, is to be founded on a soil consisting mainly of clay and sand with poor mechanical properties (see Figure 1). Natural water content is approximately 20% to 25%. An adequate functioning of such a facility is possible only if a high stability of its foundations is guaranteed. It was estimated that approximately 3000 piles would be necessary at that site. To assess the foundation performance, it was decided to perform an axial compression, pullout and flexure test in full-scale on-site condition. Fiber optic long-gage sensors were used to monitor the behavior of the six piles under test.

Long-gage fiber optic sensors have opened new possibilities for structural monitoring (1). Being long-gage, the sensors are insensitive to the local defects of materials, and therefore allow monitoring at a global, structural level. Being fiber optic based, they offer high resolution and accuracy as well as excellent long-term stability. Combined in appropriate topologies, they offer not only pure deformation (average strain) measurements, but also make it possible to determine other important parameters such as curvature, deformed shape, crack detection and localization, ultimate load capacity, Young modulus and soil properties. More than 70 sensors of this type were used for the tests.

The aim of this paper is to present the monitoring method and the results of the tests. Due to length limitations, only the most important results are presented.

DESCRIPTION OF TESTS

Two sets of reverse, cast-in place piles, respectively located on the east side and on the west side of the future facility were tested. Each set consisted of three piles, and each pile in a set was tested to a single load case, i.e. compression (according to ASTM D1143-B1), uplift (according to ASTM D3689-B3) or horizontal force (according to ASTM D3966-90). All piles had the same dimensions: a diameter of 1.20m and length of 35 m, and were designed and constructed in order to have the same mechanical properties. The compressive strength of 3 weeks old concrete samples was 24.5 MPa and calculated compression and uplift capacity was 365t and 220t respectively. The dimensions of piles, rebar layout and simplified soil mechanical properties are presented in Figure 1.

The load was applied step-wise using hydraulic jacks and according to a predetermined program. The magnitude of the applied load was monitored on the hydraulic scale of the loading set-up. Each level of load was maintained during a period whose length was determined depending on the load level. After the maximum load was reached, the piles were unloaded, again stepwise, and respecting the program.
In order to monitor the behavior of the piles during testing, each pile was instrumented with long-gage fiber optic sensors combined in appropriate topologies. In addition, the displacement of the head of the pile was recorded using LVDT-s. The measurement readings were performed immediately after each step of load and several times afterwards, while the load level was maintained. The schedule for loading as well as the schedule for the measurements is presented in Table 1. The numbers in the columns labeled "measurements" indicates the elapsed time in minutes after reaching the target load.

DESCRIPTION OF MONITORING SYSTEM

The monitoring system used in the presented tests is called SOFO (French acronym for Surveillance d'Ouvrages par Fibres Optiques – Structural Monitoring using Optical Fibers) and is based on low-coherence interferometry in optical fiber sensors (2). The functioning principle of the SOFO system is presented in Figure 2 and pictures of components can be found in Figure 3. The SOFO system consists of sensors, a reading unit and data acquisition and analysis software. The sensor consists of two optical fibers called the measurement fiber and the reference fiber and contained in the same protection tube. The measurement fiber is coupled with host structure and follows the deformations of the structure. In order to measure shortening as well as the elongation, the measurement fiber is prestressed to 0.5%. The reference fiber is loose and therefore independent from the structure's deformations; its purpose is to compensate thermal influences to the sensor. The optical signal (light) is sent from the reading unit through a coupler to the sensor, where it reflects off mirrors placed at the end of each fiber and returns back to the reading unit where it is demodulated by a matching pair of fibers. The returned light contains information concerning the deformations of the structure, which is decoded in the reading unit and visualized using a portable PC. Typical sensor length (gage-length) ranges from 200 mm to 10 m, wile the resolution reaches 2 μm independently form the gage length and with an accuracy of 0.2%. The dynamic range of the sensors is 0.5% in compression and +1.0% in elongation.
The SOFO system was developed in early 1990's and since 1995 it was commercialized and applied to the monitoring of a wide range of civil structures, such as geotechnical structures, bridges, dams, residential and industrial buildings, just to name a few (3, 4, 5, 6). The system is insensitive to temperature changes, EM fields, humidity and corrosion, and immune from drift for at least 5 years, making it ideal for both short- and long-term monitoring. Being designed for direct embedding in concrete, the sensors allow easy installation; require no calibration and feature high survival rate (better than 95% for concrete embedding). The long gage-length makes them more reliable and accurate than traditional strain sensors, averaging the strain over long bases and not being influenced by local defects in material (e.g. cracks and air pockets). More information on the SOFO system and its applications can be found in the references (6).
For the presented application, 4 m long sensors were selected. The pile was divided into eight zones (called cells). In the case of axial compression and pullout tests, a simple topology was used: the eight sensors were installed in a single chain, placed along one the main rebar, one sensor in each cell, as shown in Figure 1. To detect and compensate for a possible load eccentricity, the top cell was equipped with one more sensor installed on the opposite rebar with respect to the pile axis (see Figure 1).
In case of flexure test, a parallel topology was used: each cell contained two parallel sensors installed on two opposite main rebars, constituting two chains of sensors, as shown in Figure 1. The position of the sensors in the pile's cross-section is selected in such a way that the load direction and the sensors are aligned (see Figure 1). From the deformations measured by the sensors it was possible to calculate the average curvature of each cell, and to retrieve the horizontal displacement at each depth of the pile by double integration of measured curvatures (7).
The rebars cage of these piles was too long to be put into the borehole at once. It was therefore split into three sections, which were lowered sequentially and assembled by welding. The sensors were first installed on each section and the sensors whose position corresponded to a welded region were installed after welding, while lowering the cage. The sequence of sensor installation is schematically presented in Figure 1 and pictures taken during installation are shown in Figure 3.

AXIAL COMPRESSION AND PULLOUT TESTS: RESULTS AND ANALYSIS

The full presentation and discussion of each measured parameter largely exceeds the scope of this paper, therefore only the most significant results for each particular test are presented. The analyses and the results, which are not similar for the different tests, are mentioned but not detailed.

Average strain distribution

The average strain in each cell of a pile was determined as the ratio between the measured deformation (elongation or shortening) and the length of the sensor. This parameter served as a basis to calculate all other parameters. The distribution of the average strain over the length of the pile, in the case of the axial compression test, on the east-side pile and for increasing loads is presented in Figure 4, and for decreasing loads in Figure 5. The same diagrams obtained in the case of the pullout test are presented in Figures 6 and 7 respectively.

In Figure 4, a soil layer with poor mechanical properties was identified (encircled area). In this layer the average stain in pile is constant indicating that either the friction between the pile and the soil is low, or the stiffness / strength of the soil are low or that the cross-section of the pile is restricted. Ultrasonic test confirmed that the cross-section of the pile did not change, and therefore this anomaly is most probably due to poor mechanical properties of soil at that particular depth.

In Figure 6, a sudden increase in the strain magnitude was noticed. It was the consequence of crack formation and allowed the detection of damage (cracking) and its propagation along the pile, as a function of the load magnitude. When the maximal load was applied, cracks appeared in the first three cells.

Determination of the compressive and tensional Young modulus

The Young modulus of the pile is determined during the axial compression and pullout tests. During both tests the average strains in the first and the second cells were approximately identical for lower loads, which indicated that the soil friction in the first cell could be neglected. Hence, the Young modulus for each pile was calculated as a ratio between applied stress and average strain in the first cell. The behavior of piles under the axial compression test was linear, and the value of the Young modulus ranged from 30 GPa to 50 GPa. The piles subjected to traction had approximately bilinear or tri-linear behavior during loading and nonlinear behavior during unloading. The stress-strain diagram obtained from measurements on the east-side pile during the pullout test is presented in Figure 8. A sudden decrease in Young modulus was clearly observed after concrete cracking (compare with Figure 6).

Distribution of average normal forces

The average normal (compressive or tensile) force in the pile is determined as the product of the average strain, cross-section area and calculated Young modulus. In the case of axial compression tests, being the Young modulus constant, the compressive force distribution diagram is proportional to the one presenting the strain distribution (see Figures 4 and 5).

For the pullout test, the tensile force distribution diagram is presented in Figure 9. It has been determined taking into account the stress–strain dependence presented in Figure 8. The soil layer with poor mechanical properties was once again detected. Since its position is slightly different from that determined by axial compression test (see Figure 4), we suppose that this layer is situated in the lower part of the fourth and upper part of the fifth cell. This statement also explains the non-constant value of the force in the pile surrounded by soil with poor mechanical properties.

Determination of the ultimate load capacity and tip displacement

The ultimate load capacity of the pile subjected to compression has been determined as the minimal load causing failure of the lateral friction. It was determined as the load that significantly increases the slope on the tip force versus load diagram. When this slope significantly increases, the pile starts to slip and the tip force is activated. The slippage of the pile was also confirmed by the pile-head displacement measured by LVDT. The determination of the ultimate load capacity as well as the bottom force versus load diagram is presented in Figure 10. The bottom force was assumed to be approximately equal to the compressive force in the bottom cell.

In case of the pile exposed to traction, the ultimate uplift capacity is determined as the minimal load that damages the pile. It is clearly observed in Figure 6. This load significantly increases the slope on the pile-head vertical displacement versus load diagram, since the cracks open and the Young modulus decreases. The pile head displacement was measured using the LVDT, but was also calculated from deformations measured by fiber optic sensors. To simplify the calculation, it was assumed that the pile tip did not move. The pile head

displacement as well as the determination of the ultimate uplift capacity is presented in Figure 11. In this diagram the difference between LVDT and SOFO measurements represents the slippage of the pile.

Comparisons between calculated (predicted) bearing capacities and ultimate capacities of piles obtained from tests showed that the short-term safety factors were not satisfactory (1.32 instead 2.00 for compression and 1.56 instead 3.00 for uplift) and therefore the piles design must be changed. Both the soil-pile friction surface and the total pile traction strength must be increased.

Distribution of pile-soil friction

To simplify determination of the pile-soil lateral friction, the following assumption were adopted:

- Normal stress and strain do are constant in the pile cross-section.
- Friction is constant between the centers of neighboring cells. Consequently the normal force change is linear as well as the normal stress and strain.
- Geometrical and mechanical properties of the pile do not change with the length of pile. This assumption is necessary to simplify the analysis even if it is not entirely correct. On one hand the diameter certainly varies slightly due to the construction method and on the other hand the density of rebars is not constant over the length of the pile.

The first two assumptions are schematically represented in Figure 12.

The calculated distribution of pile-soil friction for axial compression at the ultimate load capacity (480 t) and at the maximal applied load (840 t) are presented test in Figure 13. Three zones of soil with different mechanical properties are identified and highlighted in this figure. While the first and the third zone have good mechanical properties, the mechanical properties of the second zone are significantly lower.

FLEXURE TEST: RESULTS AND ANALYSIS

Average strain in piles

During the flexure test, the order of magnitude of the average strain varied between 0με in Cell 8 and 1000με in Cell 2. The average strain with respect to load is presented in Figure 14. For practical reasons, the average strain distribution is presented with respect to the load, and not with respect to the depth of the sensor as in the case of axial compression and pullout test.

A high difference in the strain magnitude for the different Cells can be observed in Figure 14. Cell 2 was the most deformed, followed by Cells 1 and 3 while Cells 4 –8 were practically unaffected, even for the maximal applied load. For loads below 50t, parallel sensors installed in each cell measured approximately the same absolute value of deformation. This means that for those loads the pile was not cracked. For higher levels of load an asymmetry is observed due to cracking and the consequent displacement of the neutral axis.

Average curvature and displacement

The average curvature in each pile cell was calculated from the average strain assuming that the Bernoulli hypothesis is satisfied (plane cross-sections of the pile remain plane under loading) (7). The average curvature with respect to the load for the first four cells is presented in Figure 15. The curvature of the fourth cell can practically be neglected. The same is true for cells 5-8, and that's why the average curvature for these cells is not presented in the Figure 15.

The deformed shape (horizontal displacement) of pile was calculated using a double integration of the curvature function (7), and is presented in Figure 16. Again, the maximal displacement is observed in the first three cells of the pile. The point with maximal curvature in the Figure 16 corresponds to the failure point of the pile (plastic hinge).

Ultimate lateral load capacity and failure localization

The ultimate lateral load capacity of the pile was identified as the minimal load that generates cracking in the pile. According to Figures 14-16, this load is situated between 40 and 50t. The pile failed at the depth of approximately 10 m, according to Figure 16.

CONCLUSIONS

The foundation performances determined using the long-gage fiber optic sensors are resumed in Table 2. The Young modulus ranged between 45 and 50 GPa, with the exception of the east-side pile tested on compression, where the Young modulus was lower (30GPa). The maximal traction strain of concrete determined during pullout and flexure tests is approximately equal for all piles and corresponds to 60 με. The traction strength of the concrete is therefore estimated to be about 2.7-3 MPa. Since the mechanical properties were relatively uniform among all piles, it can be concluded that their quality was identical.
The tests helped to understand the real foundations behavior and to evaluate their performances, to determine failure modes and localize cracking zones and failure points. In addition mechanical properties of soil were determined and globally three layers with different properties were distinguished at both the east and the west sites. The ultimate load capacity for all tests was approximately equal to half of the maximal applied load, which is in agreement with the design values.
In future applications of the presented technique and in order to determine the Young modulus and the tip force more accurately, we recommend the use of shorter sensors (1 to 2m) in the first and last cell.

ACKNOWLEDGEMENTS

The authors of this paper would like to thank to Fu Tsu Construction Co., the contractor, as well as to Bovis Lend Lease Microelectronics, the general consultant, for their professional collaboration and kind courtesies.

REFERENCES

1. Inaudi, D., Casanova, N., Vurpillot, S., Glisic, B., Kronenberg, P., LLoret, S., *Lessons Learned in the Use of Fiber Optic Sensor for Civil Structural Monitoring*, 6th International Workshop on Material Properties and Design, Bauhaus University Weimar, Pages 79-92, September 2000, Weimar, Germany
2. Inaudi D., *Fiber Optic Sensor Network for the Monitoring of Civil Structures*, Ph.D. Thesis N° 1612, EPFL, Lausanne, Switzerland,1997
3. Inaudi D., Casanova N., *Geo-structural monitoring with long-gage interferometric sensors*, SPIE, 7th International Symposium on Smart Structures and Materials, Newport Beach, USA,Vol 3995, p 164-174, March 2000, Newport Beach, US
4. Glisic B., Badoux M., Jaccoud J.-P., Inaudi D., *Monitoring A Subterranean Structure with the SOFO System*, Tunnel Management International magazine, ITC Ltd, Vol. 2 issue 8, Pages 22-27, June 2000
5. Glisic B., Inaudi D., Kronenberg P., Vurpillot S., *Dam Monitoring Using Long SOFO Sensor*, Hydropower into the Next Century, Pages 709 - 717, October 18 - 20, 1999, Gmunden, Austria
6. www.smartec.ch
7. Vurpillot S., *Analyse automatisée des systèmes de mesure de déformation pour l'auscultation des structures*, Ph.D. Thesis N° 1982, EPFL, Lausanne, Switzerland, 1999

LIST OF TABLES AND FIGURES

List of tables

TABLE 1 Loading and measurement schedule

TABLE 2 Foundation performances determined using long-gage fiber optic sensors

List of figures

FIGURE 1 Pile dimensions, soil profile, sensor networks and sequence of installation on the rebar cages

FIGURE 2 Components and functional principle of the SOFO system

FIGURE 3 Installation of sensors on the rebar cages

FIGURE 4 Average strain distribution, for increasing loads, axial compression test, east-side pile

FIGURE 5 Average strain distribution, for decreasing loads, axial compression test, east-side pile

FIGURE 6 Average strain distribution, for increasing loads, pullout test, east-side pile

FIGURE 7 Average strain distribution, for decreasing loads, pullout test, east-side pile

FIGURE 8 Stress-strain diagram for the east-side pile under pullout test

FIGURE 9 Tensile force distribution for east-side pile under pullout test, for increasing loads

FIGURE 10 Tip force versus load diagram and determination of ultimate load capacity of the east-side pile, under axial compression test

FIGURE 11 Head displacement versus load diagram and determination of the ultimate uplift capacity of the east-side pile, under pullout test

FIGURE 12 Assumed stress and friction distribution in one section of the pile embedded in soil layer i

FIGURE 13 Distributions of the normal force in the pile, friction stress and different layers of soil

FIGURE 14 Average strain with respect to load, flexure test, west-side pile

FIGURE 15 Average curvature with respect to load, flexure test, west-side pile

FIGURE 16 Deformed shapes of the pile, flexure test, west-side pile

TABLES

TABLE 1 Loading and measurement schedule

	PULLOUT TEST		AXIAL COMPRESSION TEST		FLEXURE TEST	
Step	Load [t]	Measurement [min.]	Load [t]	Measurement [min.]	Load [t]	Measurement [min.]
0	0.0	0	0	0	0	0
1	28.6	0, 2, 5, 10	60	0, 2, 5, 10	10	0, 3, 6, 10
2	57.1	0, 2, 5, 10	120	0, 2, 5, 10	20	0, 3, 6, 10
3	85.7	0, 2, 5, 10	180	0, 2, 5, 10	30	0, 3, 6, 10, 15, 20
4	114.3	0, 2, 5, 10	240	0, 2, 5, 10	40	0, 3, 6, 10, 15, 20
5	142.9	0, 2, 5, 10	300	0, 2, 5, 10	50	0, 3, 6, 10, 15, 20
6	171.4	0, 2, 5, 10	360	0, 2, 5, 10	60	0, 3, 6, 10, 15, 20
7	200.0	0, 2, 5, 10	420	0, 2, 5, 10	70	0, 3, 6, 10, 15, 20
8	228.6	0, 2, 5, 10	480	0, 2, 5, 10	80	0, 3, 6, 10, 15, 20
9	257.1	0, 2, 5, 10	540	0, 2, 5, 10	90	0, 3, 6, 10, 15, 20
10	285.7	0, 2, 5, 10	600	0, 2, 5, 10	100	0, 3, 6, 10, 15, 20, 40, 60
11	314.3	0, 2, 5, 10	660	0, 2, 5, 10	75	0, 3, 6, 10
12	342.9	0, 2, 5, 10	720	0, 2, 5, 10	50	0, 3, 6, 10
13	371.4	0, 2, 5, 10	780	0, 2, 5, 10	25	0, 3, 6, 10
14	400.0	0, 2, 5,10, 20, 30, 40, 60	840	0, 2, 5, 10, 20, 30, 40, 60	0	0, 3, 6, 10, 15, 20
15	300.0	0, 2, 5, 10	630	0, 2, 5, 10		
16	200.0	0, 2, 5, 10	420	0, 2, 5, 10		
17	100.0	0, 2, 5, 10	210	0, 2, 5, 10		
18	0.0	0, 2, 5, 10, 20, 30, 40, 60	0	0, 2, 5, 10, 20, 30, 40, 60		

TABLE 2 Foundation performances determined using long-gage fiber optic sensors

	PULLOUT TEST	AXIAL COMPRESSION TEST	FLEXURE TEST
Young modulus of pile	E=45-50 GPa	E=30-50 GPa	Not calculated
Deformation of pile	Average longitudinal strain distribution Distribution of vertical displacement	Average longitudinal strain distribution Distribution of vertical displacement	Average longitudinal strain distribution Distribution of curvature Distribution of horizontal displacement (deformed shape)
Forces in pile	Distribution of tensile force Bottom force	Distribution of compressive force Bottom force	Qualitative distribution of bending moments
Strain when cracks occur	ε=60$\mu\varepsilon$	No crack detected	ε=60$\mu\varepsilon$
Damaging of pile	Detection of crack occurring Localization of zone affected by cracking	No damaging detected	Detection of crack occurring Localization of zone affected by cracking
Properties of soil	Qualitative determination of soil strength Identification of zones with different mechanical properties	Qualitative determination of soil strength Identification of zones with different mechanical properties	Qualitative determination of soil strength
Forces in soil	Distribution of pile-soil friction	Distribution of pile-soil friction	Distribution of horizontal reactions of soil
Failure mode	On pile (cracking)	On soil (slip)	On soil (first) and pile (afterwards)
Ultimate load capacity	314.3t to 343.2t	480t to 540t	50t

FIGURES

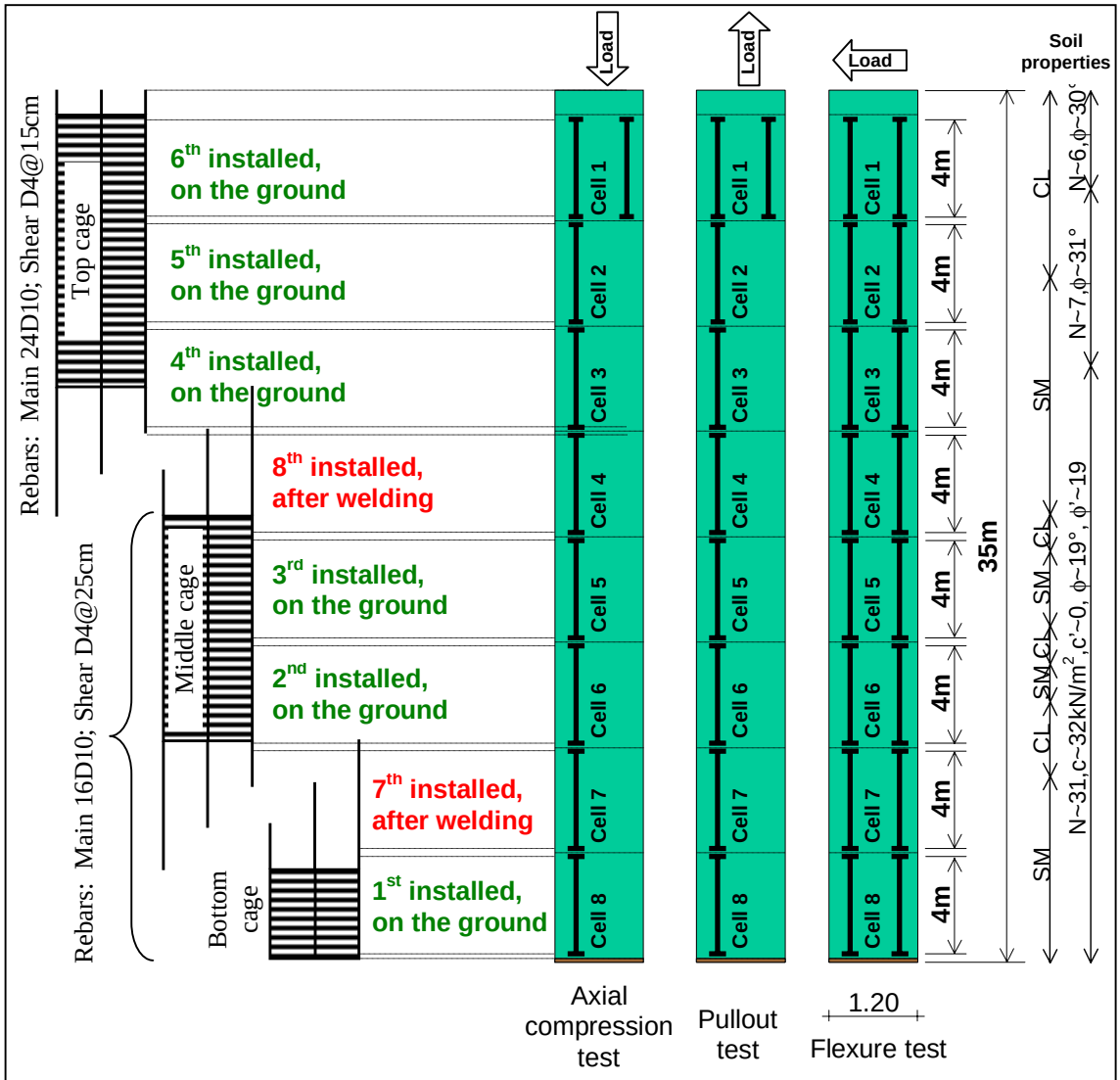

FIGURE 1 Pile dimensions, soil profile, sensor networks and sequences of installation on rebar cage

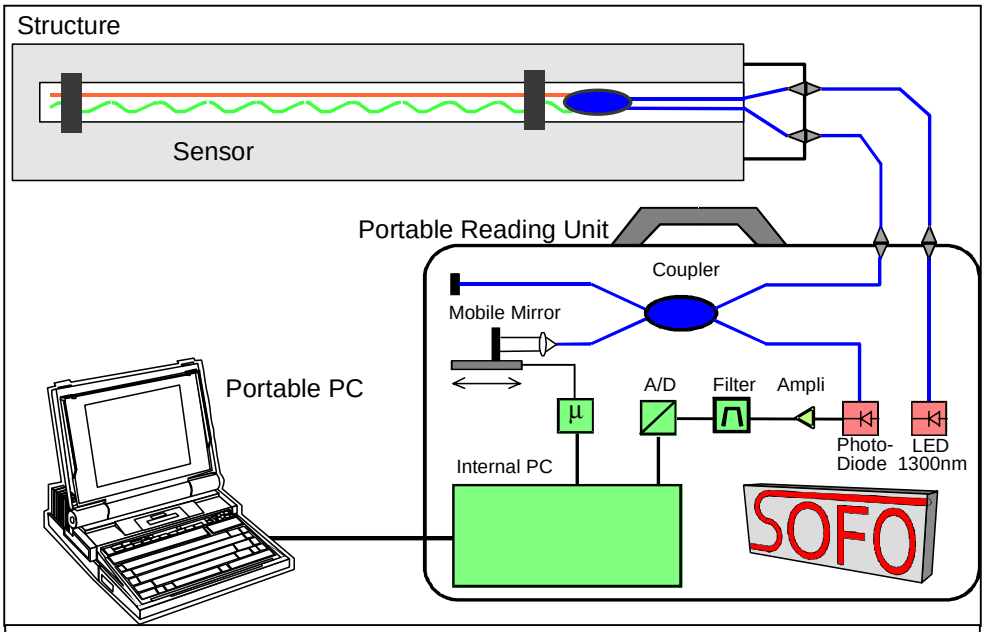

FIGURE 2 Components and functional principle of the SOFO system

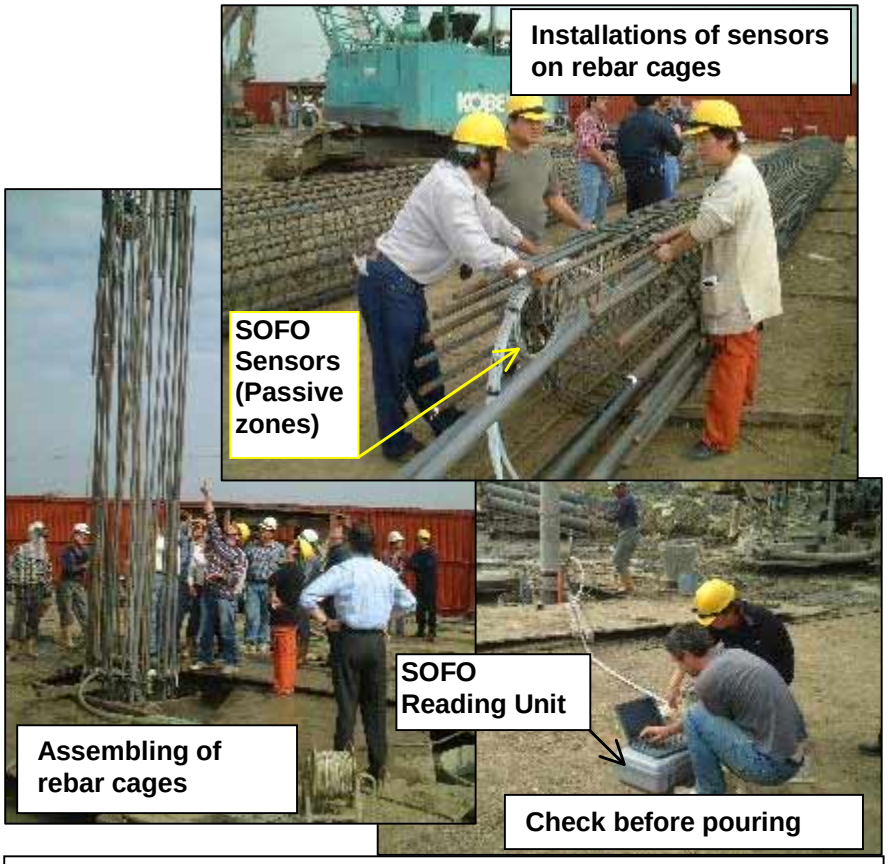

FIGURE 3 Photos taken during installation of sensors on the rebar cage

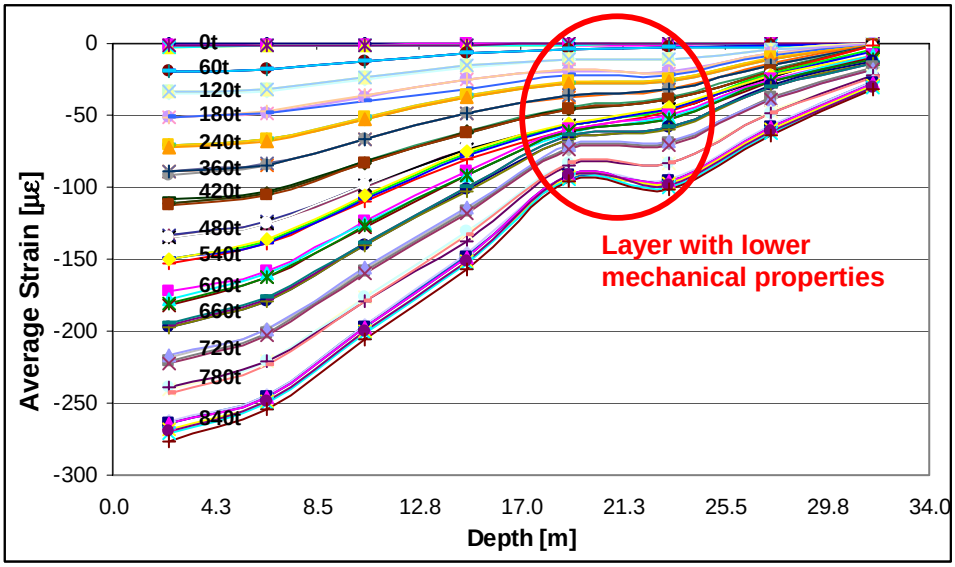

FIGURE 4 Average strain distribution, increase of load, axial compression test, east-side pile

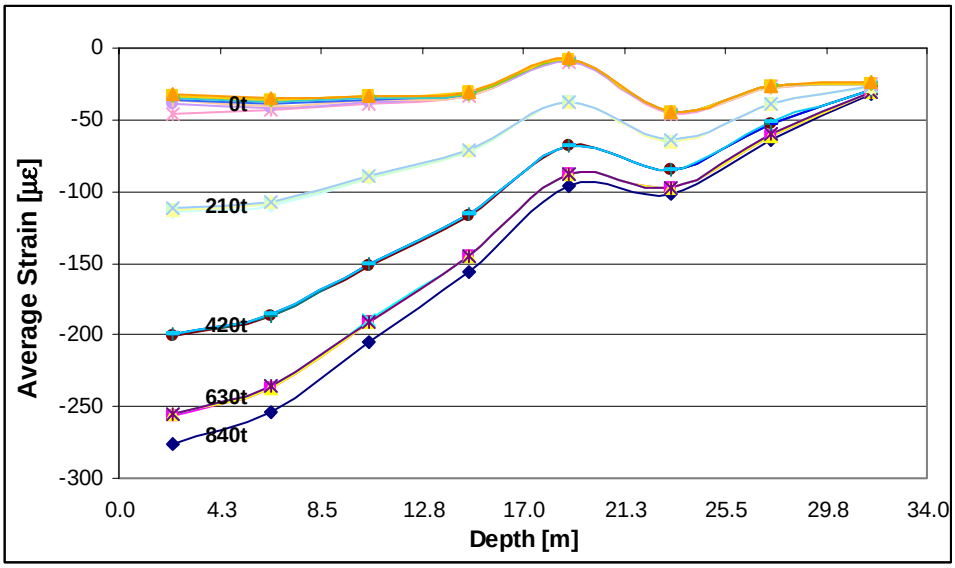

FIGURE 5 Average strain distribution, unloading, axial compression test, east-side pile

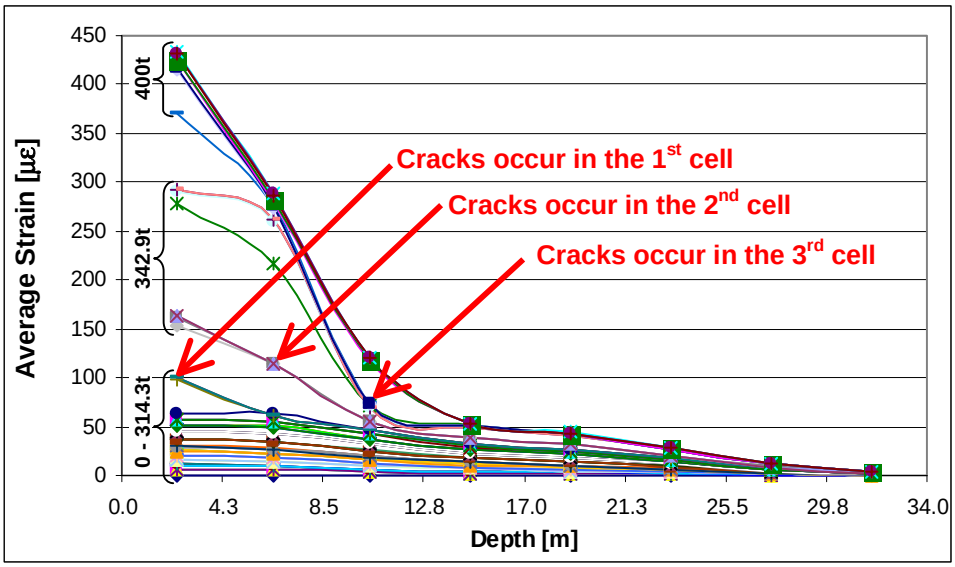

FIGURE 6 Average strain distribution, increase of load, pullout test, east-side pile

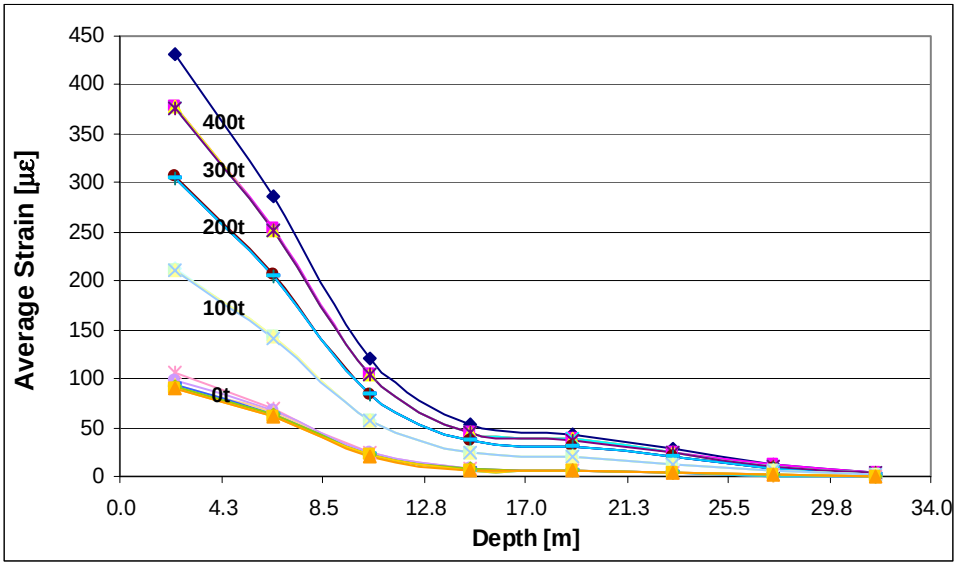

FIGURE 7 Average strain distribution, unloading, pullout test, east-side pile

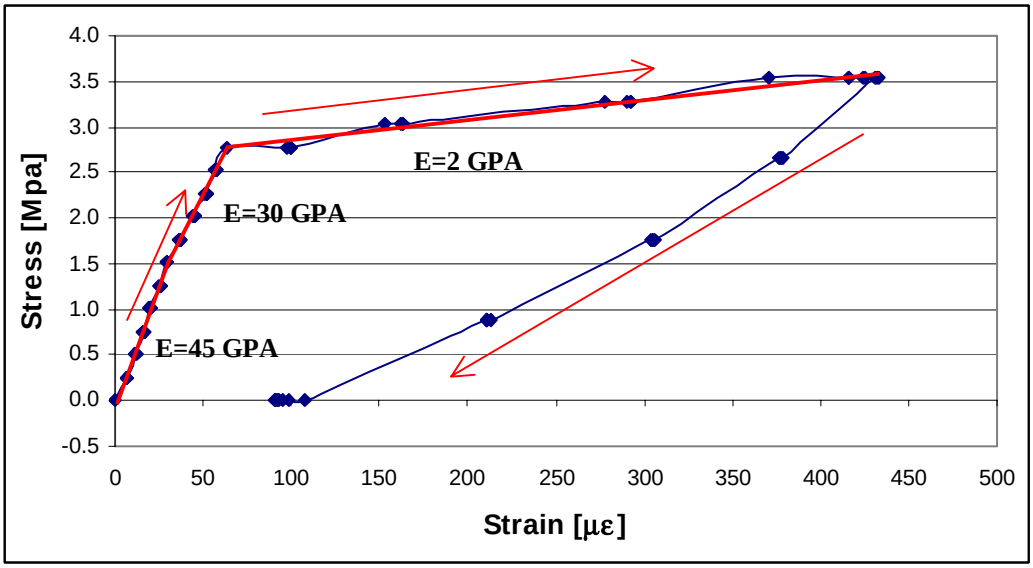

FIGURE 8 Stress-strain diagram for east-side pile under the pullout test

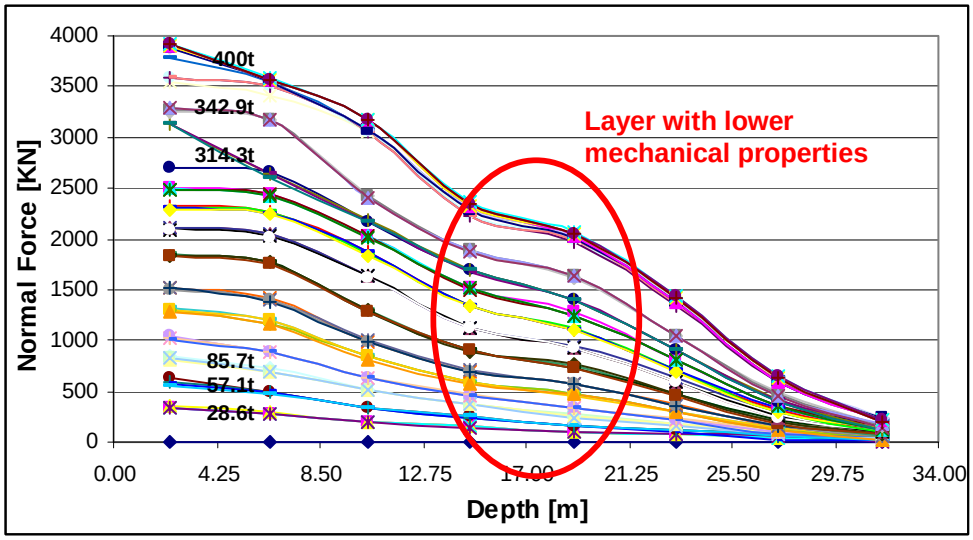

FIGURE 9 Normal force distribution for east-side pile under the pullout test, increase of load

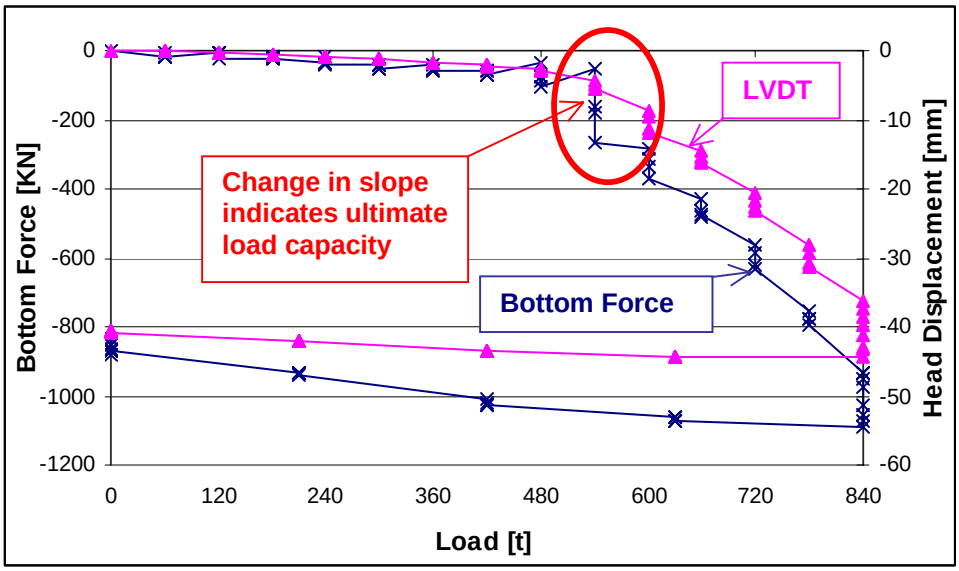

FIGURE 10 Bottom force–load diagram and determination of ultimate load capacity of the pile, east-side pile, axial compression test

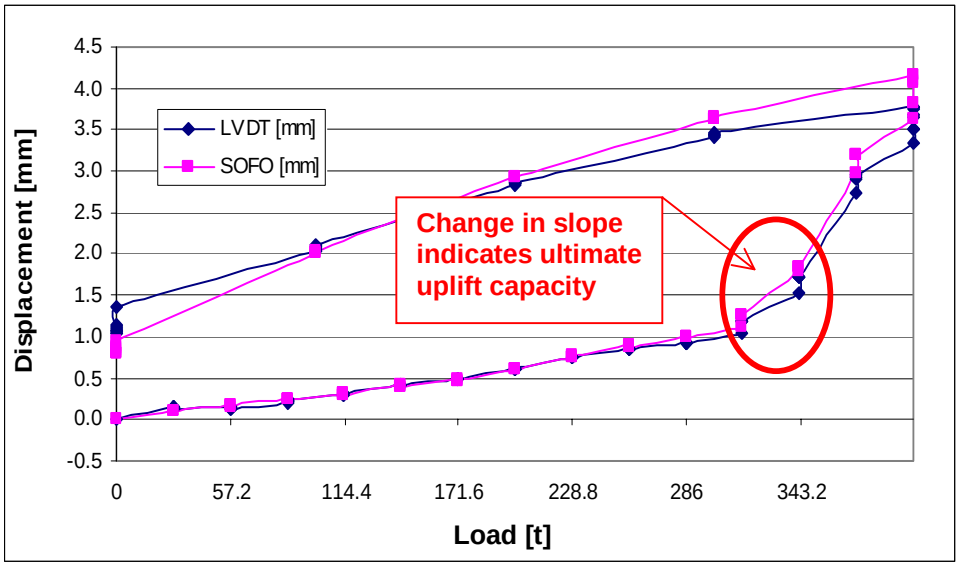

FIGURE 11 Head displacement–load diagram and determination of ultimate uplift capacity of the pile, east-side pile, pullout test

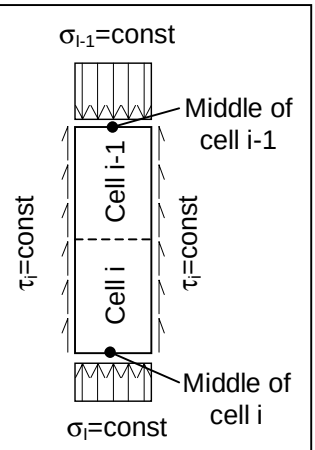

FIGURE 12 Schema of stress and friction distribution in part of pile embedded in layer i

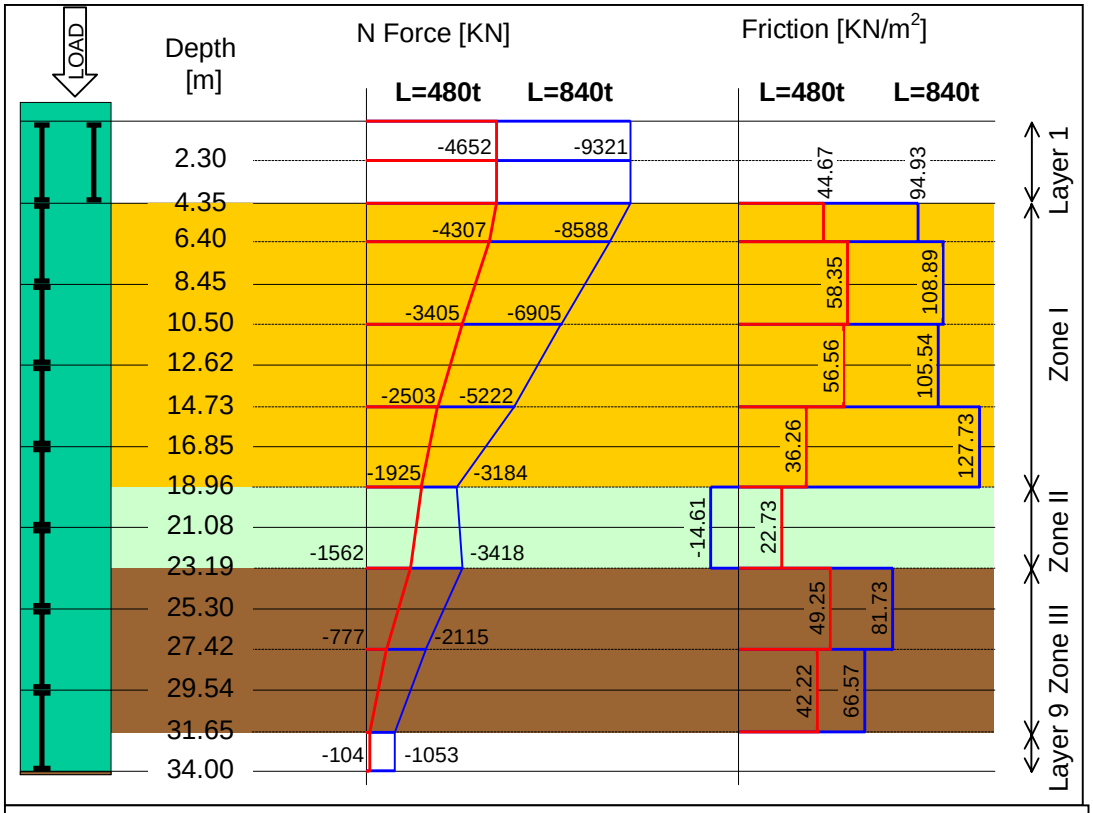

FIGURE 13 Distributions of normal force in the pile, friction stress and different zones of soil

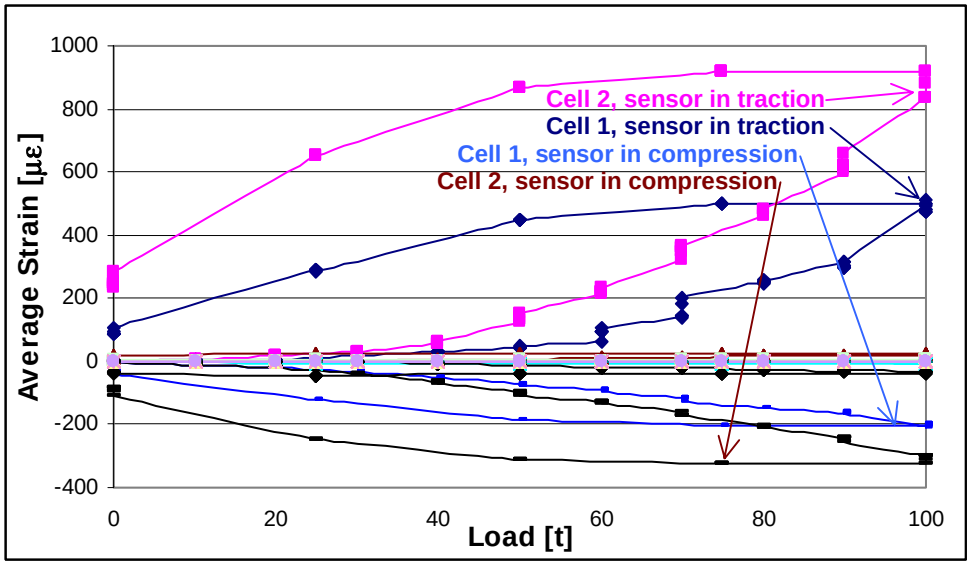

FIGURE 14 Average strain with respect to load, flexure test, west-side pile

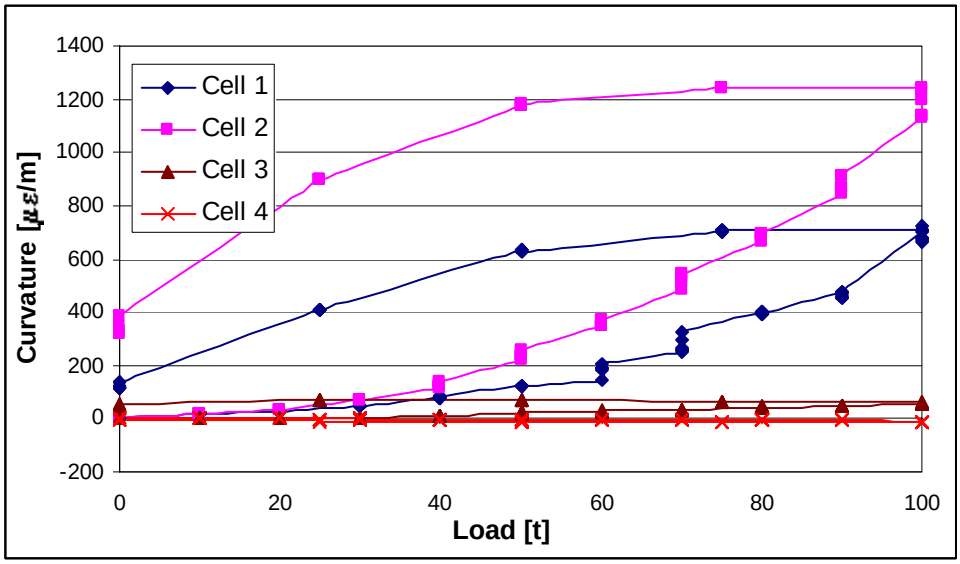

FIGURE 15 Average curvature with respect to load, flexure test, west-side pile

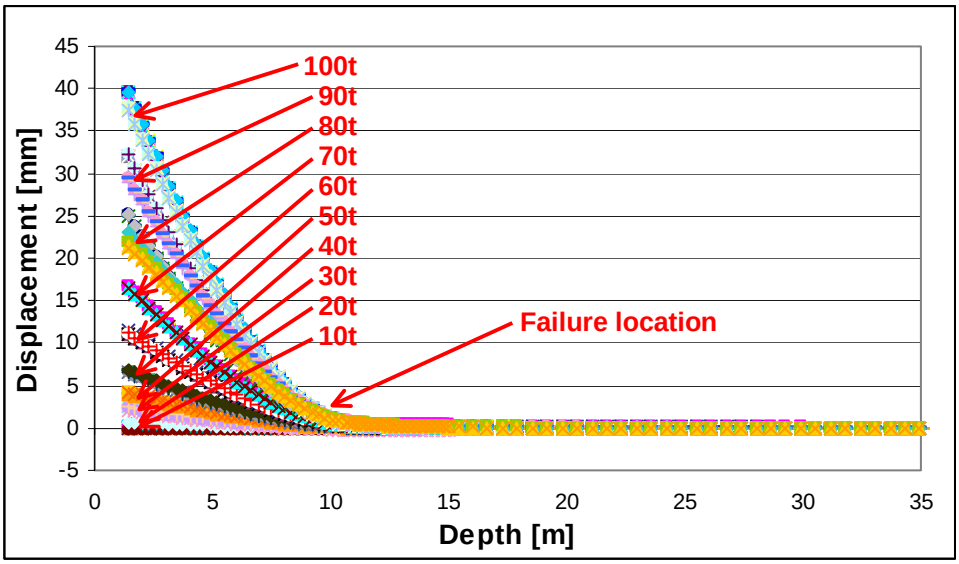

FIGURE 16 Deformed shapes of the pile, flexure test, west-side pile